Numerical Study of Normal Start and Unstart Processes In a Superdetonative Speed Ram Accelerator

Guee-Won Moon*, In-Seuck Jeung**†, Jeong-Yeol Choi***
Friedrich Seiler#, Gunther Patz#, Günter Smeets#, and Julio Srulijes#

초폭굉속도 램가속기의 정상발진과 불발과정에 대한 수치해석

문귀원* · 정인석**† · 최정렬***
Friedrich Seiler#, Gunther Patz#, Günter Smeets#, and Julio Srulijes#

ABSTRACT

A numerical study was conducted to investigate the combustion phenomena of normal start and unstart processes based on ISL's RAMAC 30 experiments with different diluent amounts and fill pressures in a ram accelerator. The initial projectile launching speed was 1.8 km/s which corresponded to the superdetonative speed of the stoichiometric H_2/O_2 mixture diluted with 5 CO_2 or 4 CO_2. Experiments with same condition except for projectile surface material demonstrated that ignition was successful with an aluminum projectile, but no combustion was observed in case of a steel projectile. In this study, it was found that neither shock nor viscous heating was sufficient to ignite the mixture at a low speed of 1.8 km/s, as was found in the experiments using a steel projectile. However, we could succeed in igniting the mixtures by imposing a minimal amount of additional heat to the combustor section and simulate the normal start and unstart processes found in the experiments with an aluminum projectile. For the numerical simulation of supersonic combustion, multi-species Navier-Stokes equations coupled with a Baldwin-Lomax turbulence model and detailed chemistry reaction equations of $H_2/O_2/CO_2$ suitable for high-pressure gaseous combustion were considered. The governing equations were discretized by a high order accurate upwind scheme and solved in a fully coupled manner with a fully implicit, time accurate integration method. The numerical results matched almost exactly to the experimental results. As a result, it was found that the normal start and unstart processes depended on the strength of gas mixture, development of shock-induced combustion wave stabilized by the first separation bubble, and its size and location.

Key Words : Ram Accelerator, Supersonic, Combustion, Detonation

1. Introduction

The concept of accelerating a projectile flying in a tube at supersonic speed by projectile-synchronized ignition of a pre-mixed combustible gas mixture, the ram accelerator, has a theoretical capability of about 10 km/s launching speed[1]. Ram Accelerator facilities offer major benefits for hypersonic research. The gasdynamic phenomena generated by ram accelerator projectiles are very similar to those expected to occur in scramjet and oblique

* 한국항공우주연구원
** 서울대학교 항공우주공학과
† enjis@snu.ac.kr
*** 부산대학교 항공우주공학과
# French-German Research Institute of Saint-Louis(ISL), Shock Tube Department

detonation wave engines. Therefore, investigating the different realms of ram accelerator operation will enhance the understanding of hypersonic propulsion phenomena in general[2,3].

Despite the number of research programs around the world during the last decade, a maximum speed of 2.7 km/s was only available at the UW (University of Washington) ram accelerator facility starting with subsonic combustion behind the projectile which was moving initially at subdetonative speeds[4]. Thus, to obtain higher velocities than 2.7 km/s, combustion must pass the transdetonative mode and finally switch into the superdetonative mode, where ignition and combustion occur at supersonic flow speeds in the space formed between projectile and tube wall.

Based on this motivation, ISL (French-German Research Institute of Saint-Louis) has developed a rail tube version of a ram accelerator facility named RAMAC 30 version II that bypassed the gasdynamic transition directly from subdetonative to superdetonative ignition. In this facility, a cylindrical projectile having conical fore- and afterbodies was launched by a powder gun and accelerated in a ram accelerator tube having four or five guide rails[5]. Although the initial launching speed of a powder gun was only about 1.8 km/s, the superdetonative launch was made possible by using the $H_2/O_2/CO_2$ mixture having a C-J (Chapman-Jouguet) detonation wave speed lower than the launching speed.

In the previous experiments, ISL's RAMAC 30 demonstrated that ignition was successful with an aluminium projectile but no combustion was observed in the case of a steel projectile. Figure 1 shows the experimental result of projectile speed according to the projectile material. After the experiment, the aluminium projectile showed ablation with significant mass loss[6]. These facts imply that there is an important ignition mechanism which is strongly related to the aluminium projectile surfaces friction, heat conduction, and combustion.

At the earlier stage of ram accelerator studies, the superdetonative mode of operation had been considered to be sustained by an oblique detonation wave positioned in the combustor. Computational studies by Yungster and Bruckner[7] and Li et al.[8] using inviscid flow model and chemical kinetics showed that ram acceleration was possible through this concept at very high velocity ranges. However, more recent viscous analyses by Yungster[9] and Choi et al.[10] showed that combustion could be initiated in the boundary layer due to the aerodynamic heating associated with shock wave / boundary layer interaction at intermediate velocity ranges where shock-heating was insufficient for mixture ignition.

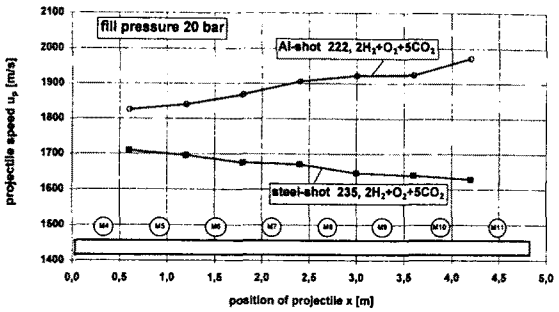

Fig. 1 Measured Projectile Velocity of Shot 222 (Aluminum Projectile) and Shot 235 (Steel Projectile)

The ISL's ram accelerator experiments, however, revealed that the previous studies on superdetonative combustion characteristics were not applicable to the experimental case and the other combustion characteristics might be more important for the low speed superdetonative mode of operation. Therefore, to understand the combustion mechanism, numerical simulations were done for ISL's RAMAC 30 experiments using the experimental configuration and mixture conditions in this study. Among the experimental cases with an aluminium projectile, shot 225 and shot 228 were selected as test cases where the former acquired best acceleration with 5 CO_2 diluent, while the latter showed an unstart process followed by a strong deceleration with 4 CO_2 diluent. The only difference between two experiments was the amount of diluent. Also, to examine the sensitivity of fill pressures of mixture, shot

224 was simulated and compared with the result of shot 225. Fill pressures of shot 224 and shot 225 was 30 bar and 40 bar, respectively.

High-pressure combustion mechanisms were employed for more accurate analyses[11] and a simple ignition model was included to simulate the experimental results. A comparison with the experimental results was made and interior ballistic combustion characteristics were interpreted from the computed flow field results.

2. RAMAC 30 Test Facility

Based on the need for a hypersonic launching facility, ISL has built two ram accelerators: a 30-mm-caliber-tube, called RAMAC 30, and 90-mm-one, RAMAC 90. The superdetonative combustion mode has been mainly tested in RAMAC 30 which was implemented with rail tube version II since 1997. Figure 2 shows the whole RAMAC 30 test facility, which consisted of a pre-accelerator tube, a ram tube containing a combustible gas mixture with both ends sealed by diaphragms which were hitted and destroyed by the moving projectile forebody nose tip, and a decelerator tube. Two tubes with a length of 2.4m each were used forming a total ram tube length of 4.8m. Projectiles had an inner magnesium core which was fully covered by an aluminium (or sometimes steel was used for different experimental shots) in the combustor as well as at the fore- and afterbodies. Cylindrical projectiles of 130g~150g, 3.0 cm caliber, and 16.1 cm long, could be accelerated to a speed of around 1800 m/s at the exit of the pre-accelerator tube before propagating through the premixture in the rail tube version II with all the equipment necessary for RAMAC 30 operation : (a) electromagnetic sensors for determination of projectile position and speed placed at the measuring stations M4 (0.3 m downstream from the ram tubes diaphragm) up to M11 (4.5 m downstream from the ram tubes diaphragm), and (b) pressure gauges for wall pressure measurement at the same measuring stations. The distance between stations was about 0.6m. In the decelerator tube at the end of the facility (c) X-ray photography and (d) a piston was located, equipped with inner replaceable steel plates for projectile catching.

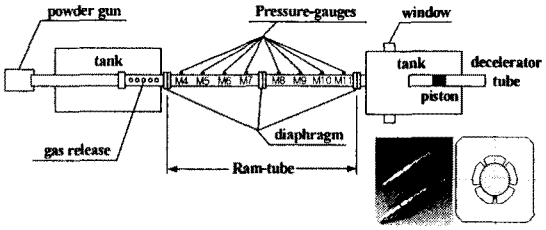

Fig. 2 Set-up of ISL's Ram Accelerator

3. Computational Modelling

3.1 Numerical Methods

In this study, a fully coupled form of species conservation equations and Reynolds averaged Navier-Stokes equations was used as a governing equation set for a chemically reacting supersonic viscous flow over an axisymmetric geometry. The governing equations for N species expressed in conservative vector form using the general curvilinear (ξ, η) coordinates are :

$$\frac{1}{J}\frac{\partial Q}{\partial t}+\frac{\partial F}{\partial \xi}+\frac{\partial G}{\partial \eta}+\frac{1}{J}H = \frac{1}{J}W+\frac{\partial F}{\partial \xi}+\frac{\partial G}{\partial \eta}+\frac{1}{J}H_v \quad (1)$$

$$F=\frac{1}{J}\begin{bmatrix}\rho_1 U\\ \rho_2 U\\ \vdots\\ \rho_N U\\ \rho uU+\xi_x p\\ \rho vU+\xi_y p\\ U(e+p)\end{bmatrix} \quad G=\frac{1}{J}\begin{bmatrix}\rho_1 V\\ \rho_2 V\\ \vdots\\ \rho_N V\\ \rho uV+\eta_x p\\ \rho vV+\eta_y p\\ V(e+p)\end{bmatrix}$$

$$H=\frac{1}{y}\begin{bmatrix}\rho_1 v\\ \rho_2 v\\ \vdots\\ \rho_N v\\ \rho uv\\ \rho v^2\\ (e+p)v\end{bmatrix} \quad Q=\begin{bmatrix}\rho_1\\ \rho_2\\ \vdots\\ \rho_N\\ \rho u\\ \rho v\\ e\end{bmatrix} \quad W=\begin{bmatrix}\omega_1\\ \omega_2\\ \vdots\\ \omega_N\\ 0\\ 0\\ 0\end{bmatrix} \quad (2)$$

Here, u, v are the velocity components in Cartesian coordinate (x,y) and U, V are the contravariant velocity in generalized coordinate. Pressure p was evaluated from the ideal gas law for a mixture of thermally perfect gases.

Although the ideal gas law may introduce some errors at high-temperature and pressure conditions, it was not considered to change the overall flow structures significantly[8]. As the Reynolds number in the ram accelerator was very high, a fully turbulent flow was assumed, and the turbulent flow was modeled by the Baldwin-Lomax eddy viscosity model[12]. This model was chosen for its simplicity and the lack of a sufficiently accurate model for this kind of flow. In turbulent premixed flames, severe fluctuations between burnt and unburnt gas may occur and computing the chemical source terms using a mean temperature may lead to wrong results. To avoid the mean reaction rate problem, direct numerical simulation or statistical approach using the probability density function(PDF) is an attractive methods which are not yet applicable to this kind of complex flow[13]. Therefore, the interaction between turbulence and chemistry was not considered in this study. Previous reduced kinetics mechanisms were based mainly on low-pressure(1atm) data, whereas ram accelerators typically operate at pressures much greater than 50atm. Therefore, the finite-rate chemistry models should include high-pressure effects where applicable. Petersen and Hanson[14] developed reduced mechanisms to model the combustion characteristics of typical ram accelerator mixtures at pressures approaching 300 atm based on the GRI-Mech. Thus, we adopted a fully detailed, 10-species and 29-step reaction model for the combustion of $H_2/O_2/CO_2$ mixture. The species considered are H, H_2, O, O_2, OH, H_2O, HO_2, H_2, O_2, CO and CO_2. This reaction mechanism is a subset of GRI-Mech. 2.11 that includes the pressure dependent reaction formulation[11,15] for several reactions above. The finite volume cell-vertex scheme was used for spatial discretization of governing equations. The viscous terms were discretized by central difference and the convective terms were expressed as differences of numerical fluxes at cell interface. The numerical fluxes containing artificial dissipation were formulated using Roes FDS(Flux Difference Splitting) method[16]. MUSCL (Monotone Upstream Method for Scalar Conservation Law) scheme[17] was used for the extrapolation of primitive variables at cell interface. The discretized equations were solved by a fully implicit, time integration method based on a LU-SGS scheme[18]. Detailed description of numerical algorithms has been documented in a previous work[10].

3.2 Numerical Modelling

Diameters of a projectile and a tube shown in Fig. 2 was 3.0 cm and 4.2 cm, respectively. In the experiment, the tube wall had a decagonal cross-section with five rails but was assumed circular for the axisymmetric simulations. Initial launching speed was set to 1,800m/s from the experiment and assumed constant during computation. Initially the mixtures for shot 225 and shot 228 had a pressure and temperature of 40 bar and 300K, respectively. The gas composition used for shot 225 was $2H_2 + O_2 + 5CO_2$: a stoichiometric H_2/O_2 mixture diluted with 5 moles of CO_2. For shot 228, however, the amount of diluent was reduced to 4 moles of CO_2 to make it more energetic. In case of shot 224, the only difference compared to shot 225 was the fill pressure of 30 bar.

T × 100 computational grid that was uniformly distributed in the axial direction and clustered to both walls in the radial direction. Since these simulations had to cover overall flow features of the scale of the entire projectile, the computational resolutions used were limited. Therefore, details of the detonation structure, such as the induction region, might not be well resolved. But our purpose was exploring the overall development and so, current grid resolution was enough to represent the shock and detonation position because the local transit time was sufficiently smaller than the induction time of $2H_2 + O_2 + 5CO_2$mixture computed after the reflected shock where mixture ignition occurred. he computational domain for the current simulation was extended by 1cm before and after the projectile, and it was covered by the 380

The no-slip boundary condition was applied at both the projectiles surface and the tube

wall. The tube wall was considered isothermal and the projectiles surface adiabatic. There was a temperature gradient at the tube wall, but none at the projectiles surface. The zeroth-order extrapolation method was used for out-flow boundary conditions and the symmetric condition was used along the axis of symmetry. Steady state solution of the frozen flow for this condition was used as an initial condition for the reactive flow simulation.

4. Results

4.1 Preliminary Results without Forced Ignition

Figure 3 presents the numerical results for shot 225 without any forced ignition mechanism. For the frozen flow result in Fig. 3 (a), the pressure contours show that a regular shock reflection pattern and a separated flow region was formed at the projectiles surface from shock wave / boundary layer interaction. It is readily understood that the separated flow region will be a point of self-ignition due to the high temperature by flow stagnation.

Reactive flow solution in Fig. 3 (b) starting from the frozen flow solution shows burnt gas region bounded by a strong temperature gradient. Combustion generated by thermal dissipation was largely confined to the thin combusting layer near the projectiles surface and didn't ignite the flow outside the boundary layer. So, the combustion region started from the enlarged separated flow region and extended to the exit remaining as a boundary layer flame.

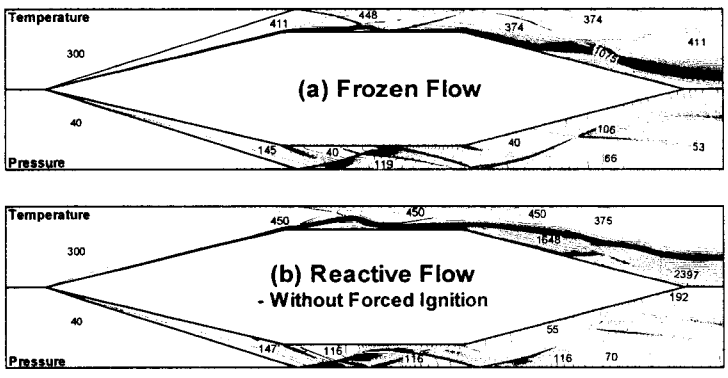

Fig. 3 Temperature and Pressure Contours from Numerical Simulation of Shot 225 without Any Forced Ignition Mechanism. (a) Frozen Flow, (b) Reactive Flow.

The high pressure(520bar) behind the conical reflected shock didn't induce detonation due to relatively low temperature(570K) behind it, since the chemical reaction rates are largely controlled by the local temperature, and to a lesser extent by the local pressure. Although the separated boundary layer induced shock waves which might have influence on the oblique-detonation structure, the strength of the separation-induced shock was weak and it was not focused with the conical reflected shock. Also the combustion along the boundary layer didnt induce detonation because expansion waves were generated between the separation bubble and reattached shocks. Apparently, the heat transfer from the thin combusting layer near the projectiles surface to the main flow seemed to be insignificant. As such, this case does not produce any thrust and the combustion mode corresponds to that of upper dilution limit unstart[8].

Even though this result does not agree with the experiments using an aluminium-covered projectile, it is guaranteed by the ISL's experimental results with a steel-covered projectile where no detonation and hence, no thrust is produced[4]. Therefore, it implies that ignition mechanisms of shock heating or viscous heating cannot explain the results of experiments with an aluminium projectile travelling at 1.8 km/s. This means that another ignition mechanism may be present at the relatively low speed of 1.8 km/s for the superdetonative mode of operation. This mechanism should be related to the properties of the

aluminium projectile which is easier to melt and burn than the steel projectile.

In the ISL's RAMAC 30 configuration, there may be two friction mechanisms. One is the friction between the aluminium projectiles surface and mixture and the other is between its surface and the guide rails. Although the viscous heating is not sufficient to ignite the $H_2/O_2/CO_2$ mixture, it is enough to melt the aluminium surface yielding molten aluminium particles which may be blown into the stream. In addition, there is the metallic friction between the surface and rails that may heat the aluminium surface above the ignition temperature of the mixture. Thus, the projectile might have already been heated well beyond the melting point of the aluminium, the mixture ignition temperature, or the aluminium ignition temperature.

Anyway, the friction mechanisms could initiate the surface burning of the aluminium projectile to yield sufficient heat to initiate detonation of the combustible gas, even though the contribution of the heat addition by aluminium surface combustion was insignificant.

4.2 Forced Ignition Modelling

Even if we neglect the combustion of aluminium at particle phase, the mathematical modelling should include the aluminium surface combustion. But, we assumed that the aluminium surface burning contributed just to initiate detonation in the ram accelerator and consequently modelled it by imposing a small amount of heat on the flow field. The location and amount of heat addition were previously investigated and we imposed a minimal amount of additional heat to the front of the combustor to initiate the detonation[15]. On the x-ray picture which was taken in the decelerator tube, strong ablation took place at the mid- and afterbody of the aluminium projectile[6]. But it doesn't mean where ignition occurred. Strong ablation was due to the intensive combustion after ignition.

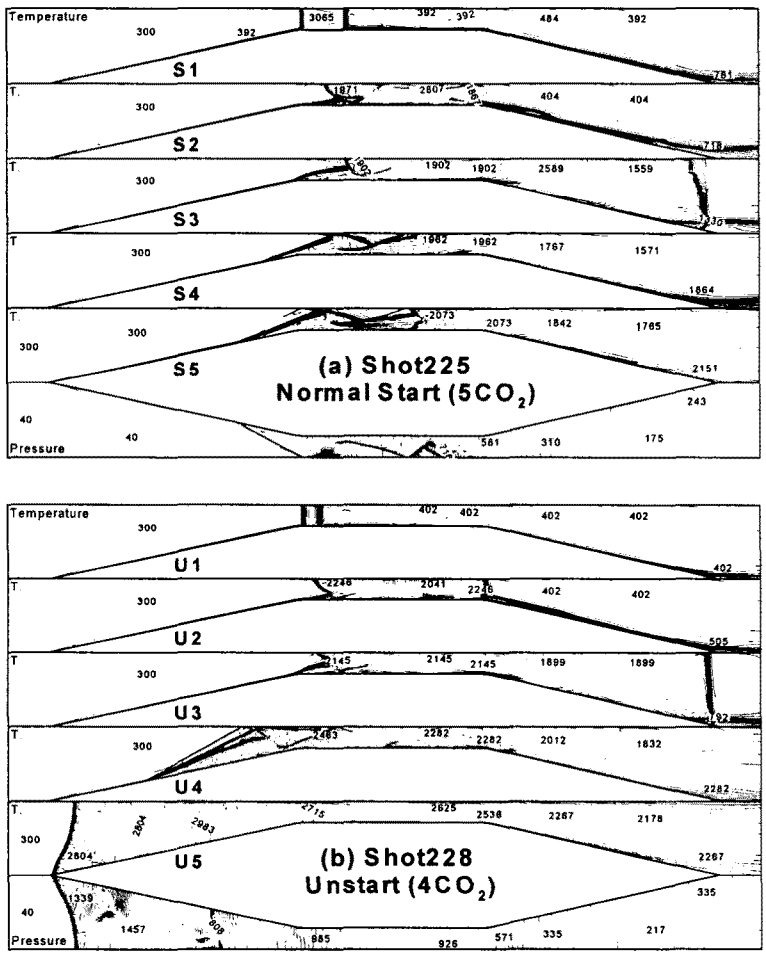

Fig. 4 Initiation and Evolution of Detonation with External Ignition Source.
(a) Normal Start with 2H2+O2+5CO2 (shot 225)
(b) Unstart with 2H2+O2+4CO2 (shot 228)

4.3 Initiation and Evolution of Detonation in the Normal start and Unstart Processes

Figure 4 shows the numerical results of shot 225(5 CO_2) and shot 228(4 CO_2) which demonstrated normal start and unstart process according to the diluent composition, respectively. At an earlier stage of ignition, the flame front was created perpendicular to the tube wall by the ignition energy. In case of shot 228 with more energetic mixture, ignition energy imposed on the front section of combustor was 1/4 the amount of shot 225(Fig. 4 (a) S1, Fig. 4 (b) U1). As time proceeded, the flame front interacted with the conical shock which was reflected on the tube wall. The reflected shock and reaction front created a large separation bubble just forward of the interaction point at the projectile surface. But, the flame between projectile and tube wall was forced to move downstream by supersonic flow for both cases because the flame front was not strongly sustained(Fig. 4 (a) S2, Fig. 4 (b) U2). The flame of shot 228 with a relatively strong mixture was coupled to the reflected shock front and hence a detonation was formed near the tube wall. In case of shot 225 the location of detonation was same in the beginning but it was forced to move downstream, where the reflected shock and separation-induced shock were focused due to a relatively weak mixture(Fig. 4 (a) S3, Fig. 4 (b) U3). As the separation bubble grew, the separation-induced shock had more strength.

Therefore, the focusing point of reflected shock and separation-induced shock moved ahead of the detonation wave, where a strong shock-induced combustion was occurred. Accordingly, the detonation wave of shot 225 was forced to move downstream by supersonic flow because the flame front was not strongly sustained(Fig. 4 (a) S4). In case of shot 228, strong shock-induced combustion was occurred where the separation-induced shock was reflected as the separation bubble grew and moved upstream. But initially formed detonation wave looked stationary because of the energetic mixture, although it gradually weakened by expansion waves behind the separation bubble(Fig. 4 (b) U4).

Finally, the flame front of shot 225 was blown off downstream near the tube wall and strong reattached / reflected shock created a second separation bubble at the projectile surface. The edge of the separation bubble acted as a flame front around the projectile surface, while detonation was formed near the tube wall where the strong reattached shock was reflected. Accordingly, the whole flame structure became stable and continuous acceleration was plausible with the $2H_2 + O_2 + 5CO_2$ mixture(Fig. 4 (a) S5). In case of shot 228 the separation bubble near the shoulder greatly enlarged and moved upstream. Furthermore, the combustion wave, basically driven by a very strong shock-induced combustion, also traveled upstream in front of the projectile. The projectile now moved into a high pressure flow field sustaining high drag forces, called unstart, followed by a strong projectile deceleration(Fig. 4 (b) U5)

4.4 Comparison between Experiment and Numerical Simulation

4.4.1 Tube wall pressure

Figure 5 shows the comparison of wall pressures among the experiments and corresponding numerical simulations of shot 224(30bar, 5 CO_2), shot 225(40bar, 5 CO_2) and shot 228(40bar, 4 CO_2) after a flight of 1.5m from the ram tubes diaphragm(M6 station). It is apparent that the numerical results matched almost exactly to the experimental results in terms of magnitudes and location for three cases and this fact confirms the practicability of our analysis about the interior ballistic mechanisms of normal start and unstart processes from the computed flow field results. The results of shot 224 and shot 225 showed normal acceleration with similar flame structure even though the magnitude of acceleration was different according to the fill pressure. The pressure of shot 225 at the projectile wall which is important to thrust, was higher than that of shot 224 over the whole flow field. This is because the mixture strength of shot 225 was stronger as the fill

pressure was increased.

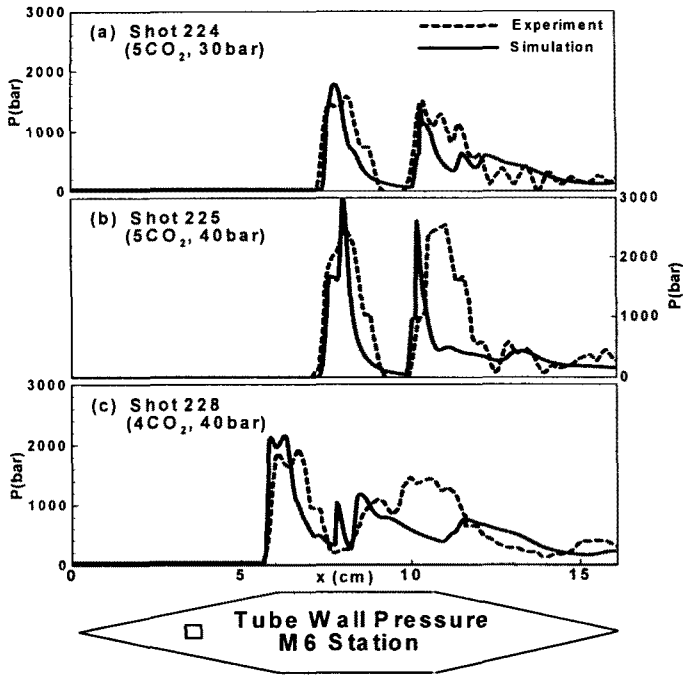

Fig. 5 Comparisons of Tube Wall Pressure between Experiment and Corresponding Numerical Simulation
(a) Normal Start with 2H2+O2+5CO2 and 30 bar (shot 224)
(b) Normal Start with 2H2+O2+5CO2 and 40 bar (shot 225)
(c) Unstart with 2H2+O2+4CO2 and 40 bar (shot 228)

In order to analyze the relationship between the wall pressure and the combustion mechanisms in a ram accelerator, schematics are presented in Fig. 6. Figure 6 (a) represents the flow result S4 of Fig. 4 (a), while Fig. 6 (b) is from the flow results U4 of Fig. 4 (b). In the tube wall pressure curve of Fig. 6 (a), (a1) is 40 bar, the initial mixture pressure in the ram tube, (a2) represents the pressure of about 1700 bar raised by the incident / reflected shock combined with the separation-induced shock and its associated reflected shock. After that, pressure is decreased to about 1500 bar by expansion waves generated in front of the separation bubble. The pressure peak (a3) corresponding to about 2900 bar is due to a strong shock-induced combustion and considered as a Von Neumann spike. After the pressure peak, pressure is decreased considerably due to strong expansion waves behind the separation bubble. Point (a4) shows the pressure increased to 950 bar by combination of a reattached and associated reflected shock produced by compression waves behind the separation bubble. The pressure is modestly stationary due to the expansion waves generated from the combustion wave but second pressure peak of 2600 bar (a5) appears again due to a normal detonation wave. Behind the detonation wave, the pressure level is decreased to about 600 bar, denoted by (a6), as a result of the expansion accompanied behind the detonative combustion. Fig. 6 (b) of shot 228 can be understood in the same way, noting that the first separation bubble stabilized at the projectiles nose cone is considerably larger than its counterpart in Fig. 6 (a).

4.4.2 Acceleration

Figure 7 (a) shows the experimental acceleration calculated from the mean velocities between two neighboring stations[6] and Fig. 7 (b) is the computational acceleration from the thrust force that is given from the gas pressure acting on the projectiles surface. In Fig. 7 (b) S3S5 and U3U5 correspond to the evolution stages of Fig. 4 (a) and Fig 4 (b), respectively.

The experimental data of station M10 for shot 225 was excluded because it was measured at the stage of severe ablation due to the strong heat flux directed from hot and compressed gas flow into the cold projectiles surface. Therefore, the experiment of shot 225 got positive acceleration and the computed results coincided with that of the experiment. Both the experiment and simulation of Shot 228 were in good agreement : unstart followed by a strong deceleration.

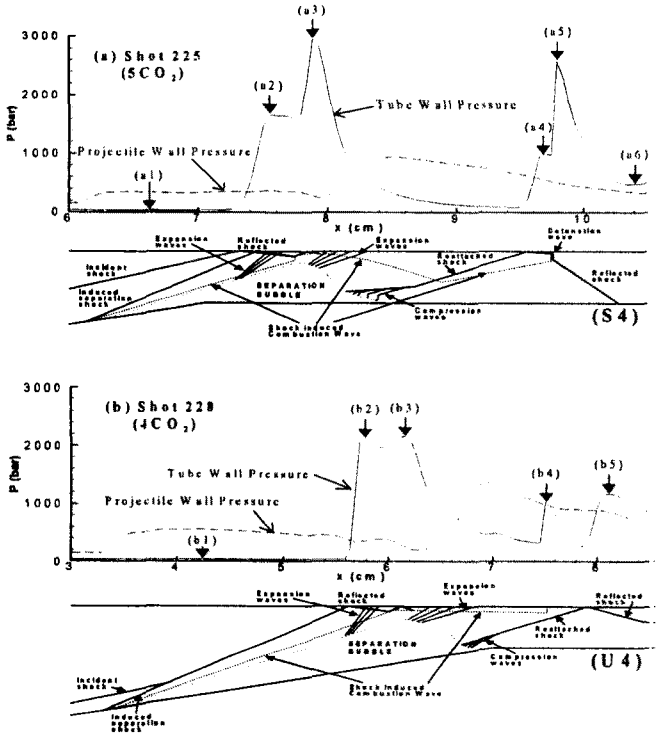

Fig. 6 Tube Wall Pressures and Corresponding Schematics of Interior Ballistic Combustion Mechanism
(a) Normal Start with 2H2+O2+5CO2 (shot 225)
(b) Unstart with 2H2+O2+4CO2 (shot 228)

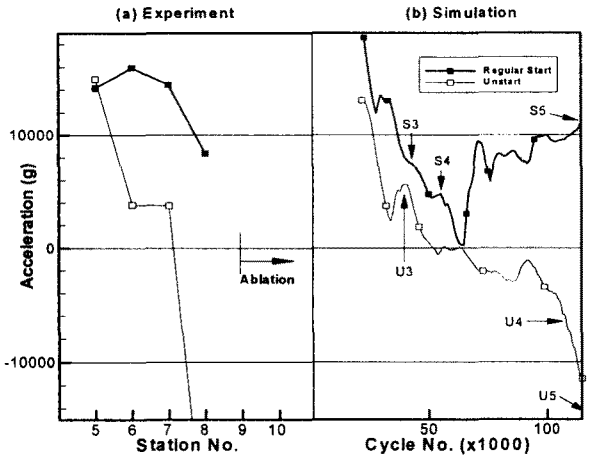

Fig. 7 Comparisons of Acceleration between Experiment and Numerical Simulation
(a)Experimental Result, (b)Numerical Simulation Result

5. Conclusion

Based on the investigation of the combustion mechanisms in ISL's RAMAC 30 experiments, a numerical study was carried out with a simple model of the ignition mechanism. By imposing additional heat initially in the model, we could simulate the normal start of shot 224, shot 225 and unstart of shot 228. From these results, it was found that the normal start and unstart processes depended on the strength of gas mixture, development of shock-induced combustion wave stabilized by the first separation bubble, and its size and location.

This means that if the mixture is energetic, the initial detonation wave is stationary, although gradually weakened by expansion waves behind the separation bubble. Accordingly the first separation bubble grows continuously and the combustion wave will travel upstream in front of the projectile. The projectile moves in a high pressure flow field producing high drag forces on the projectile, called unstart, followed by a strong deceleration.

On the other hand, if the mixture is weak such that the initial detonation wave is forced to move downstream near the tube wall, strong reattached / reflected shock waves create a second separation bubble which retards the growth of the first separation bubble while maintaining a stable flame structure. As a result, continuous acceleration is possible and leads to a normal start process.

The fact that the calculated tube wall pressure matched well to their experimental counterparts in terms of magnitudes and location, makes it possible to understand the interior ballistic combustion mechanisms of normal start and unstart processes from the flow field results.

References

[1] Hertzberg, A., Bruckner, A.P., and Bogdanoff, D.W., AIAA Journal, Vol. 26, No. 2, pp. 195-203 (1988).

[2] Bruckner, A.P., and Knowlen, C., National Shock Wave Symposium, Sendai, Japan, 1993.

[3] Bogdanoff, D.W., Journal of Propulsion and Power, Vol. 8, No. 2, pp.481-490 (1992).

[4] Elvander, J.E., Knowlen, C., and Bruckner, A. P., Ram Accelerators, Springer-Verlag, pp.55-64, 1988.

[5] Seiler, F., Patz, G., Smeets, G., and Srulijes, J., Second International Workshop on Ram Accelerators, Seattle, WA, 1995.

[6] Seiler, F., Patz, G., Smeets, G., and Srulijes, J., AIAA Paper 98-3445, Cleveland, OH, 1998.

[7] Yungster, S., and Bruckner, A. P., Journal of Propulsion and Power, Vol. 8, No. 2, pp.457-463 (1992).

[8] Li, C., Kailasanath, K., and Oran, E. S., Combustion and Flame, Vol. 108, pp.173-186 (1997).

[9] Yungster, S., AIAA Journal, Vol. 30, No. 10, pp.2379-2387 (1992).

[10] Choi, J.-Y., Jeung, I.-S., and Yoon, Y., AIAA Journal, Vol. 36, No. 6, pp.1029-1038 (1998)

[11] Choi, J.-Y., Lee, B.-J. and Jeung, I.-S., Journal de Physique IV, Vol.10, Pr.11, pp.131-141(2000).

[12] Baldwin, B. S., and Lomax, H., AIAA Paper 78-257, Jan. 1978.

[13] Riggins, D. W., Drummond, J. P. and Carpenter, M. H., Gas Turbine Combustion V.1, von Karman Institute for Fluid Dynamics Lecture Series 1990-02, 1990.

[14] Petersen, E.L. and Hanson, R.K., Journal of Propulsion and Power, Vol. 15, No. 4, pp.591-600 (1999).

[15] Moon, G.-W., Jeung, I.-S., Choi, J.-Y., Yoon, Y., Seiler, F., Patz, G., Smeets, G., and Srulijes, J., Journal de Physique IV, Vol.10, Pr.11, pp.143-153(2000).

[16] Roe, P. L., Journal of Computational Physics, Vol. 43, pp. 357-372 (1981).

[17] Hirsch, C., Numerical Computation of Internal and External Flows, Vol. 2, John Wiley & Sons, New York, 1990.

[18] Shuen, S. and Yoon, S., AIAA Journal, Vol. 27, No. 12, pp. 1752-1760 (1989).